NANO LETTERS

pubs.acs.org/NanoLett

Letter

Digital Magnetic Detection of Biomolecular Interactions with Single Nanoparticles

Sanyou Chen,[#] Ziting Sun,[#] Wanhe Li,[#] Pei Yu,[#] Qian Shi, Fei Kong, Qi Zhang, Pengfei Wang, Ya Wang, Fazhan Shi,[*] and Jiangfeng Du[*]

Cite This: *Nano Lett.* 2023, 23, 2636−2643

Read Online

ACCESS | Metrics & More | Article Recommendations | Supporting Information

ABSTRACT: Biomolecular interactions compose a fundamental element of all life forms and are the biological basis of many biomedical assays. However, current methods for detecting biomolecular interactions have limitations in sensitivity and specificity. Here, using nitrogen-vacancy centers in diamond as quantum sensors, we demonstrate digital magnetic detection of biomolecular interactions with single magnetic nanoparticles (MNPs). We first developed a single-particle magnetic imaging (SiPMI) method on 100 nm-sized MNPs with negligible magnetic background, high signal stability, and accurate quantification. The single-particle method was performed on biotin−streptavidin interactions and DNA−DNA interactions in which a single-base mismatch was specifically differentiated. Subsequently, SARS-CoV-2-related antibodies and nucleic acids were examined by a digital immunomagnetic assay derived from SiPMI. In addition, a magnetic separation process improved the detection sensitivity and dynamic range by more than 3 orders of magnitude and also the specificity. This digital magnetic platform is applicable to extensive biomolecular interaction studies and ultrasensitive biomedical assays.

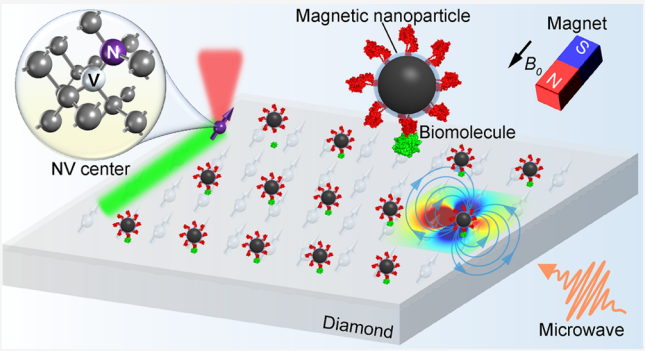

KEYWORDS: *Magnetic imaging, Nitrogen-vacancy center, Biomolecular interaction, Digital detection, Immunomagnetic assay*

Biomacromolecules interact to coordinate physiological processes in cells and organisms. There are numerous *in vivo* methods for studying cellular biomolecular interactions,[1,2] providing a wealth of knowledge about biomolecular functions. For *in vitro* detection of interactions, elaborately designed biosensors and platforms are essential.[1,3,4] For instance, surface plasmon resonance[5] and biolayer interferometry[6] have been rapidly developed for label-free detection of biomolecular interactions. In addition, single-molecule methods such as single-molecule fluorescence detection,[7,8] single-molecule force spectroscopy,[9] and nanopore detection[10] are widely used to measure biomolecular interactions at the single-molecule level, greatly expanding our understanding of biomolecules. However, many of them rely on optical detection, which usually suffers from optical background, signal instability, light scattering, and fluorescence blinking.

Magnetism-based approaches are promising candidates for overcoming the challenges associated with optical detection.[11] In most of these approaches, magnetic nanoparticles (MNPs) used as labels or tools offer many unique advantages, including a near-background-free property, high signal stability, magnetic manipulation capacity, accessible functionalization, and magnetic penetrability, which make them attractive for a wide range of biomedical applications.[11] There are various magnetometry techniques for detecting MNPs,[12,13] such as giant magnetoresistance (GMR) sensors,[14] superconducting quantum interference devices, and Hall effect sensors. Among these techniques, GMR sensors have been used to measure the kinetics of protein interactions.[15] However, all of the above sensors have difficulty resolving a single MNP with a 100 nm scale or smaller size. A magnetic biosensor that can resolve single MNPs with high throughput would realize highly efficient magnetic detection of biomolecular interactions with single-molecule sensitivity, which is a challenge for conventional techniques.

Magnetic detection using nitrogen-vacancy (NV) centers in diamond provides a conceptual solution for this goal.[16] The NV sensor has already presented powerful capabilities in the high-sensitivity detection of magnetic fields.[17−21] Moreover, the biocompatibility of diamond and sensing capabilities under ambient conditions render NV centers ideal sensors for

Received: December 20, 2022
Revised: March 24, 2023
Published: March 27, 2023

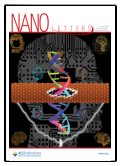

https://doi.org/10.1021/acs.nanolett.2c04961
Nano Lett. 2023, 23, 2636−2643

applications in biomedical systems. These features and advances have attracted much interest in single-molecule structure research,[22−24] single-cell imaging,[25−27] tumor tissue imaging,[28,29] biomagnetism sensing,[19] and DNA assay,[30] indicating the prospects of NV-based magnetic sensing in extensive biomedical fields. In particular, a 15 pT/Hz$^{1/2}$ sensitivity[19] and a 10 nm-scale spatial resolution[27] have been achieved. Although some experiments using NV centers recently imaged single magnetic particles,[31,32] the lack of biofunctionalization and the poor detection efficiency hindered their biomedical applications. To date, meaningful magnetic sensing attempting to detect biomolecular interactions remains elusive.

Here, integrating the superiorities of NV sensors and MNPs, we establish a digital magnetic method to detect biomolecular interactions based on single-particle magnetic imaging (SiPMI) using 100 nm-sized magnetic particles. In addition, many biomedical assays, such as enzyme-linked immunosorbent assay (ELISA)[33,34] and paper microfluidic lateral flow assay (LFA),[35] utilize specific biomolecular interactions to qualitatively or quantificationally examine target molecules and diagnose a state. In this work, we also introduce a digital immunomagnetic assay based on SiPMI for examining severe acute respiratory syndrome coronavirus 2 (SARS-CoV-2)-related antibodies and nucleic acids.

PRINCIPLE AND CONCEPTUAL DESIGN

Figure 1A shows a conceptual design of single-particle magnetometry for detecting biomolecular interactions. Single MNPs are brought to the diamond surface by interacting biomolecules and examined by SiPMI to qualitatively and quantificationally analyze the interaction. In this work, SiPMI detects single MNPs not necessarily single molecules. Nonetheless, because one pair of interactional molecules is sufficient to connect an MNP to the diamond, SiPMI can achieve single-molecule detection. For specific biological recognition, the diamond and MNP surfaces are prefunctionalized (see the Supporting Information). Multiple biomolecules conjugated on a single MNP enable highly efficient interactions. Moreover, as will be explained later, SiPMI can detect as low as a single MNP.

To sense the MNPs, the optically detected magnetic resonance (ODMR) experiment of magnetic imaging was carried out in a diamond-based magnetic microscope with a spatial resolution of ∼400 nm (Figure 1 and the Supporting Information). As the principle, the continuous-wave (CW) spectrum of NV centers is measured to calculate the magnetic field. Specifically, static magnetic field B shifts the peak position of the CW spectrum by a magnitude of $\gamma_e B$ due to the Zeeman effect (Figure 1B, C).[17] In our experiments, $B = B_0 + B_{MNP}$, where B_0 is the externally applied magnetic field along an NV axis, which also magnetizes MNPs. At each imaging pixel, the local magnetic field projection of an MNP, B_{MNP}, affects the peak position by a magnitude of $\gamma_e B_{MNP}$ (Figure 1C). Therefore, the local magnetic field of a single MNP can be obtained by measuring the frequency shift of NV centers and subtracting the external magnetic field B_0. In the magnetic microscope, single MNPs on the diamond surface are imaged in a field of view (FOV) of hundreds of micrometers by a two-dimensional (2D) thin layer of NV sensors with a detection sensitivity of ∼2 μT·μm/Hz$^{1/2}$ (Figure 1A). The magnetic fields are mapped pixel-wisely in a wide-field manner.

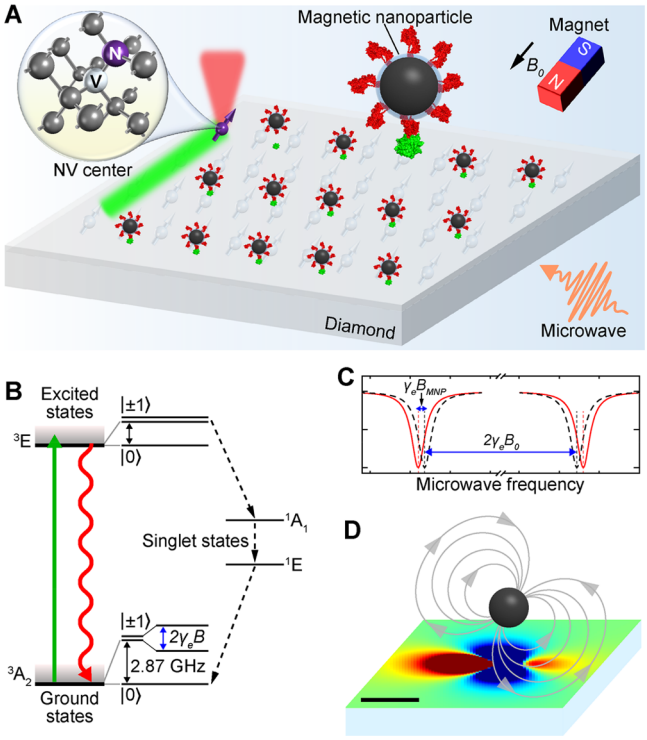

Figure 1. Schematic illustration and principle of single-particle magnetic detection for biomolecular interactions. (A) Illustration of SiPMI detection. Biomolecule (red)-coated MNPs specifically bind on the diamond surface by interacting with preimmobilized biomolecules (green). Single MNPs are magnetized by an external magnetic bias field B_0 and imaged by a 2D magnetic sensor, which consists of many shallow NV centers in the bulk diamond. The NV centers are excited by a green laser (532 nm) and modulated by a microwave field, and the red fluorescence is collected to read the NV spin state. The single-particle magnetic image is used to analyze the interaction. The inset shows the atomic structure of an NV center. (B) Energy-level diagram of the NV center. Zero-field splitting degenerates the ground states $|0\rangle$ and $|\pm1\rangle$ with 2.87 GHz. Under magnetic field B, the energy level of $|\pm1\rangle$ splits due to the Zeeman effect, which is proportional to B ($\Delta = 2\gamma_e B$, for NV gyromagnetic ratio, γ_e, of 2.80 MHz/gauss). In the excited states, $|\pm1\rangle$ states partially relax to the ground state of $|0\rangle$ through the singlet states, which is a nonradiative transition. (C) CW spectra of NV centers. The peak appears in the CW spectrum when the microwave frequency is resonant with the allowed transition $|0\rangle \rightarrow |-1\rangle$ or $|0\rangle \rightarrow |+1\rangle$. (D) Simulated magnetic image of a single MNP on the diamond surface. Scale bar, 500 nm.

In this study, superparamagnetic nanoparticles with an average diameter of 100 nm were selected to reconcile appropriate magnetic field strength and high throughput in the single-particle imaging and magnetic manipulation capacity. On the diamond surface, the estimated distance between the MNP surface and the NV layer is approximately 40 nm, which is determined by the NV depth of ∼20 nm and molecules coated on the diamond and MNP surfaces. Simulated images show that a single MNP displays a distinctive pattern of a petaloid magnetic dipole field with a typical magnetic magnitude of 25 μT and micrometer-scale spatial extension (Figures 1D and S1). These enable us to image MNPs with high contrast and single-particle resolution while permitting many MNPs in an FOV. In principle, we can spatially resolve up to 10,000 single MNPs in an FOV of 100 × 100 μm^2. In addition, the ability of magnetic separation in ∼1 min allows

https://doi.org/10.1021/acs.nanolett.2c04961
Nano Lett. 2023, 23, 2636−2643

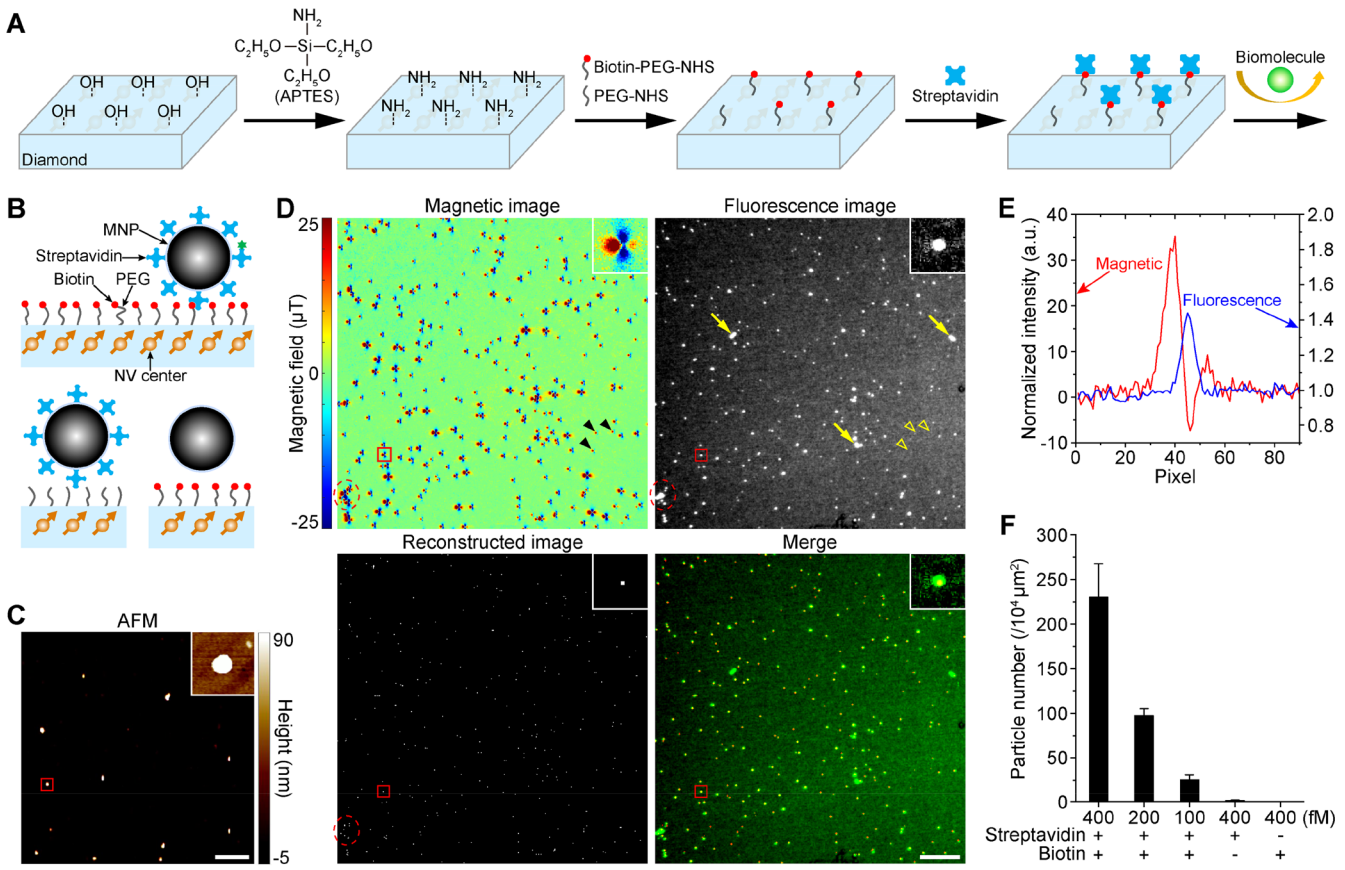

Figure 2. Proof-of-concept experiments of SiPMI detection. (A) Workflow of modification and functionalization of the diamond surface (see the Supporting Information for details). The SA modification allows subsequent binding of biotin-terminated biomolecules. (B) Schematic of biotin−SA interaction detection. Biotin-PEG molecules are preimmobilized on the diamond surface, and then, SA-coated MNPs bind on the surface via the biotin−SA interaction. The green star indicates the fluorophore Alexa Fluor 488 (AF488) labeled on the SA. Groups using methyl-terminated PEG (mPEG)-modified diamond or carboxyl-terminated MNPs served as controls. (C) AFM image of single MNPs binding on the diamond surface via the biotin−SA interaction. The MNP concentration was 400 fM. The inset shows a single MNP. (D) Correlated single-particle magnetic and fluorescence images. The fluorescence image shows AF488 labeled on the corresponding MNPs. The distribution of MNPs was reconstructed from the magnetic image by a deep learning model. Insets show magnified images of the single MNP in red boxes. Yellow arrows indicate autofluorescence structures. Arrowheads indicate MNPs that appear in the magnetic image but cannot be found in the fluorescence image. Red ellipses represent an MNP cluster. (E) Linear profile analysis of single-particle signals. The analyzed MNP is the particle in the magnified images in (D). a.u., arbitrary units. (F) Quantification of MNP numbers per 10,000 μm^2. Values on the abscissa represent concentrations of MNPs. Data are represented as mean ± SEM, $n \geq 4$ areas for each group. Scale bars: (C) 2 μm; (D) 10 μm.

rapid pre-magnetic purification and enrichment for biomedical samples. To accurately identify and reconstruct single-particle magnetic field signals, we trained a deep learning model based on the pix2pix method, an image-to-image translation framework.[36] As a result, the single MNPs can be intelligently recognized by the trained model and subsequently accurately counted (Figure S2).

MAGNETIC DETECTION OF BIOTIN−STREPTAVIDIN INTERACTION

We first performed the single-particle method in a model system of the biotin−streptavidin (SA) interaction (Figure 2). As the first key issue, nonspecific binding (NSB) disturbs many biomedical assays.[37] Although the chemically inert diamond surface largely avoids NSB, we still observed moderate NSB of SA and obvious NSB of MNPs at high concentrations (Figures S3A and S4). To minimize the NSB of biomedical samples and MNPs, optimizing the diamond surface is critical. In our experiments, the modification and PEGylation of the diamond surface successfully eliminated the NSB and enabled subsequent specific biofunctionalization and single-molecule/particle detections (Figures 2, S3, and S4), which were also achieved with Al_2O_3-coated diamonds in a recent work.[38]

On the biotinylated PEG-functionalized diamond, SA-coated MNPs specifically bound on the surface via the biotin−SA interaction (Figure 2B). In addition to dispersing the MNPs in the solution (Supporting Information), we also optimized their concentration to obtain a spatially resolvable distribution. At a subpicomolar concentration, the MNPs were distributed on the diamond surface with a distance of several micrometers between each other (Figure 2C, D). The atomic force microscopy (AFM) image confirmed the single-particle distribution (Figure 2C). In the correlated magnetic and fluorescence microscope, we obtained the single-particle magnetic image as well as the single-particle fluorescence image of fluorophores labeled on corresponding MNPs, which confirmed the magnetic signals of single MNPs (Figure 2D). Note that the heterogeneity of single-particle magnetic signals primarily arises from the fluctuation of particle size (Supporting Information).

In general, magnetic detection is free from the impact of background signals, as there is barely a magnetic background in

https://doi.org/10.1021/acs.nanolett.2c04961
Nano Lett. 2023, 23, 2636−2643

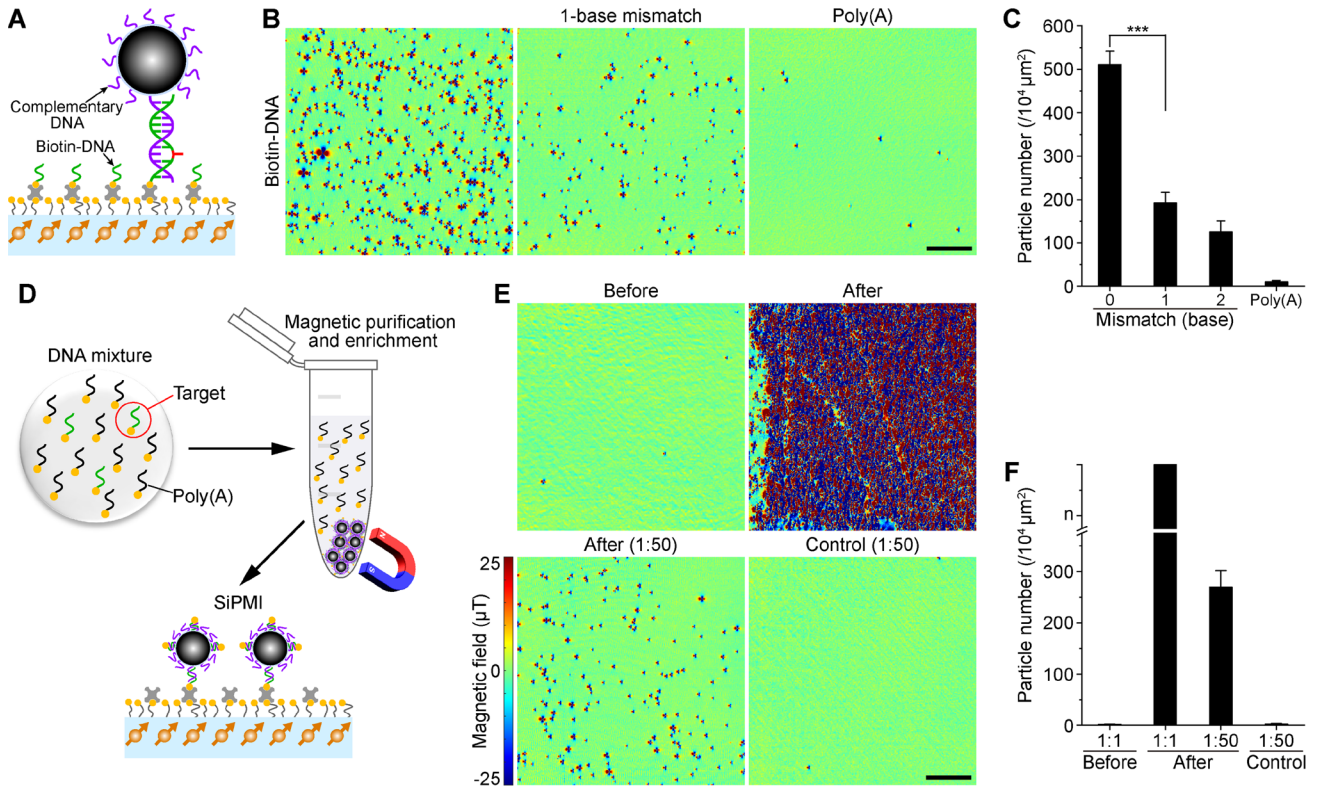

Figure 3. SiPMI detection of DNA oligo hybridization. (A) Schematic of DNA−DNA interaction detection. Biotin−DNA molecules are immobilized on the diamond surface via SA. An assumptive mismatch base is marked in red. (B) Single-particle magnetic images of DNA oligo hybridization. In the three groups, the complementary DNA strand was constant, but the biotin−DNA strand had a variable sequence with no mismatch, one-base mismatch, or poly(A). (C) Quantification of MNP densities. The particle density has a significant downward trend as the number of mismatched nucleotides is increased, indicating the decrease of interaction strength. Data are represented as mean ± SEM, $n \geq 5$ areas for each group. ***$P < 0.001$, t test. (D) Schematic of magnetic purification and enrichment followed by SiPMI detection. The DNA mixture consisted of target biotin−DNA (10 pM) and biotin-poly(A) (100 nM). Complementary DNA-coated MNPs (1 pM) were added into the mixture and fully reacted. The reaction solution was concentrated from 1 mL to 5 μL by magnetic separation. Then, the sample was examined by SiPMI. (E) Single-particle magnetic images of samples before or after magnetic separation. Images were from undiluted samples (upper) or samples with a 50-fold dilution after magnetic separation (lower). In particular, the treatment procedure of the control group was the same as that described in (D), except that the target biotin−DNA was excluded from the DNA mixture. (F) Quantification of MNP densities in (E). We cannot count the exact particle number of the after (1:1) group because of the excess MNPs in the FOV. Data are represented as mean ± SEM; $n \geq 5$ areas for each group. Scale bars, 20 μm.

biomedical samples and detection systems. In contrast, fluorescence detection usually suffers from background fluorescence, as the larger spots indicated by the yellow arrows in Figure 2D. Obviously, magnetic imaging has a much better signal-to-background ratio than fluorescence imaging in the same imaging system (Figure 2D, E) and excellent magnetic signal stability relative to fluorescence signals (Figure S5). To quantitatively analyze the interaction, we employed the trained deep learning model to identify the single-particle magnetic fields and reconstructed them as single-particle magnetic moments with a nearly 100% reconstruction rate (Figure 2D). The deep learning scheme facilitates the recognition of single MNPs, including the segmentation of magnetic signals that overlap or are from a cluster (as the cluster indicated by the red ellipses in Figure 2D), which greatly improves the quantification accuracy. Moreover, the characteristic magnetic dipole pattern of single MNPs further minimizes the false identification of background signals, such as the spurious signal in Figure S2B, which does not present a typical pattern and can be explained by the presence of internal strain or surface damage in the diamond. These features collectively guarantee the robustness and accuracy of the single-particle method.

Furthermore, we investigated the relationship between magnetic signal density and MNP concentration and found that the particle density was proportional to the concentration (Figure 2F). The lack of signal in the negative control groups without biotin or SA confirmed that the single-particle signals were from biotin−SA interactions rather than NSB and other factors.

DNA OLIGO HYBRIDIZATION

Biomolecular interactions involving nucleic acids widely exist in DNA replication, DNA repair, transcription, translation, gene editing, and various biomedical assays.[39,40] Here, we used SiPMI to detect DNA oligo hybridization. Due to the apparent electronegativity, DNA molecules easily bound nonspecifically on bare diamonds primarily through electrostatic adsorption (Figure S6). We found that PEGylation almost completely eliminated the nonspecific adsorption of DNA on diamonds (Figure S6). As shown in Figure 3A, the complementary strand conjugated on the MNP interacted with the single strand preimmobilized on the diamond surface. SiPMI results clearly reveal the sequence specificity of DNA hybridization, and the particle density is markedly reduced in the mismatch groups

https://doi.org/10.1021/acs.nanolett.2c04961
Nano Lett. 2023, 23, 2636−2643

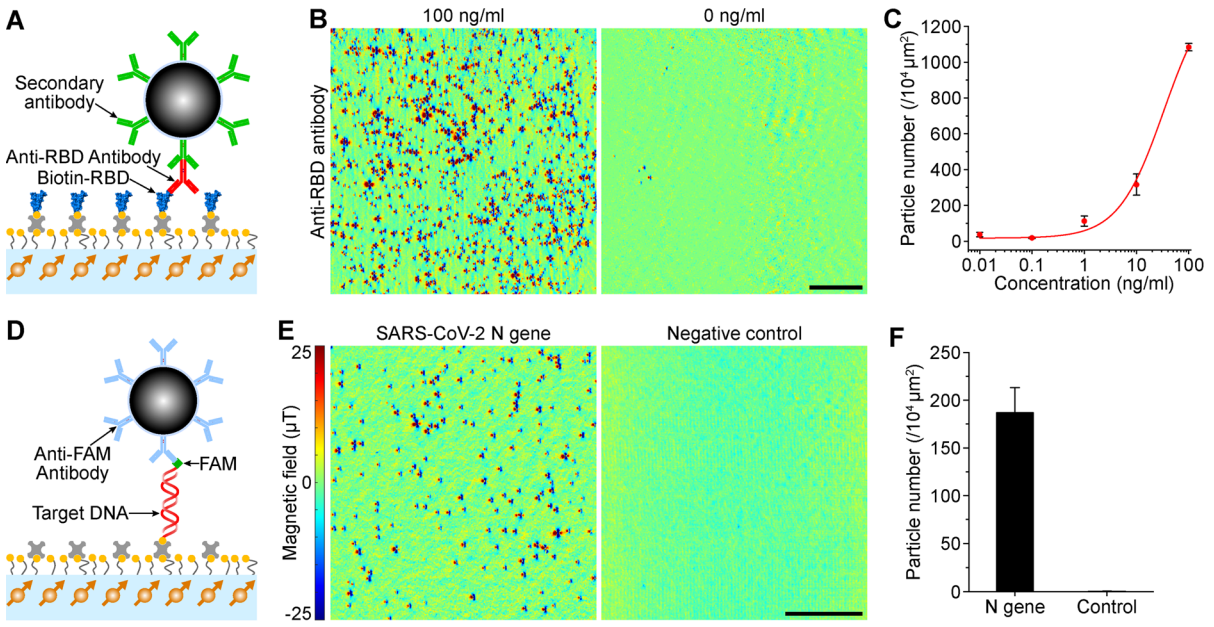

Figure 4. (A–C) Single-particle immunomagnetic assay of SARS-CoV-2-related antibodies. (A) Schematic of the SPIMA. In the sandwich structure, biotinylated RBD proteins, which are used as capture molecules, are immobilized on the SA-functionalized diamond surface. The target molecule anti-RBD antibody is captured via the antigen–antibody interaction. The secondary antibody-conjugated MNP is used to recognize the primary antibody and detect the protein interaction. (B) Single-particle magnetic images with or without anti-RBD antibodies in the sample. (C) Concentration-dependent curve of the immunomagnetic assay for the anti-RBD antibody. Data are represented as mean ± SEM; $n \geq 5$ areas for each group. (D–F) The SPIMA of SARS-CoV-2-related nucleic acids. (D) Schematic of the assay. The SARS-CoV-2 N gene in a plasmid was amplified by LAMP (Supporting Information). 175-bp DNA duplexes in the amplicon were the target of the assay. 5′-Fluorescein (FAM)-modified and 5′-biotin-modified primers were used in the amplification to produce labeled double-stranded amplicons, which bound to the anti-FAM antibody-coated MNP and the SA-modified diamond, forming a sandwich structure in the presence of amplicons. (E) Single-particle magnetic images. The two samples were from the LAMP reactions with 10,000 copies of the SARS-CoV-2 N gene as the template or without template (negative control). (F) Quantification of MNP densities in (E). Data are represented as mean ± SEM; $n \geq 5$ areas for each group. Scale bars, 20 μm.

and the control group of poly(A), which have reduced interaction strengths (Figure 3B,C). Significantly, SiPMI detection is single-base sensitive for the DNA–DNA interaction. This sensitivity to mismatches makes SiPMI detection an ideal way to detect sequence variants of interest relevant to various diseases and biomedical elements, such as the cancer genome, genome of a novel viral strain, a single nucleotide polymorphism genotype, and noncoding RNA.

Magnetic separation is an important characteristic of magnetic particles.[41] Here, we investigate the potential of magnetic purification and enrichment based on magnetic separation in improving the sensitivity and specificity of SiPMI detection. For this purpose, single MNPs were used as both tools for magnetic separation and signal resources for magnetic imaging. After the incubation of MNPs and the DNA mixture (biotin-poly(A):target biotin–DNA = 10,000:1), the target DNA oligo was coprecipitated and examined by SiPMI (Figure 3D). Not only does poly(A) interact weakly with complementary strands on MNPs, but also excess biotin-poly(A) severely disturbs the tethering of target DNA on the diamond by occupying the biotin-binding sites of SA. As a result, in addition to enhancing the specificity, the magnetic separation process improved the sensitivity and dynamic range of SiPMI detection by more than 3 orders of magnitude, which was calculated based on the 50-fold dilution factor and the approximately 100-fold higher particle density of the diluted "After" group compared to the "Before" group and the "Control" group (Figure 3E,F). The results of the control group without target DNA excluded nonspecific signals caused by increased MNPs after the concentration (Figure 3E,F). These expanded abilities of the single-particle method will provide new opportunities for biomedical applications, especially for low-abundance molecules and complex content-containing samples such as blood, urine, saliva, and cell or tissue extract.

PROTEIN INTERACTION AND IMMUNOMAGNETIC ASSAY

Protein–protein interactions occur almost all the time in all biological systems and also are the biological basis of many immunoassays.[1,42] We further applied single-particle magnetic detection to the antibody–antigen interaction, a representative protein interaction, and established a single-particle immunomagnetic assay (SPIMA), which is one of the digital detection strategies widely used in ultrasensitive analytical assays.[34,43−45] There is an urgent requirement for highly sensitive diagnostic tests, especially during the coronavirus disease 2019 (COVID-19) pandemic.[46] Here, as a proof-of-concept assay, the SPIMA was first employed to detect an antibody against the receptor-binding domain (RBD) of the SARS-CoV-2 spike protein. As the sandwich structure shows in Figure 4A, biotin–RBD proteins used as capture molecules were preimmobilized on the diamond surface, and secondary antibody-coated MNPs were used to recognize and probe the target molecules anti-RBD antibodies. Single-particle magnetic field signals were observed when there were anti-RBD antibodies in the sample, and the particle density was concentration dependent; but, only a few isolated signals were observed in the control group

https://doi.org/10.1021/acs.nanolett.2c04961
Nano Lett. 2023, 23, 2636−2643

without target molecules (Figure 4B,C). In the groups with low sample concentrations, the SPIMA had single-molecule detection. Except for the limitation of the dissociation constant of the interactional biomolecules, the unremarkable limit of detection (LOD) here could be improved by increasing the capture rate of the target molecules on the diamond surface and further reducing the NSB level of the entire detection system. In addition to the SARS-CoV-2 antibody, we have also shown the SPIMA for the loop-mediated isothermal amplification (LAMP)-based amplified product of the SARS-CoV-2 N gene (Figure 4D−F), demonstrating the broad applicability of the approach. Benefiting from the high specificity and single-MNP sensitivity of the SPIMA, the target nucleic acids were specifically identified despite skipping the purification of amplicons. The effectiveness of the SPIMA for real clinical samples has also been proved by testing the SARS-CoV-2-induced antibody in the serum of a convalescent patient with COVID-19 (Figure S7).

The SPIMA shows the practical value of the single-particle method, and the approach can be readily modified to study general protein−protein interactions at the single-molecule level or further developed into an ultrasensitive clinical assay approach. Owing to the near-background-free property and the single-particle sensitivity of SiPMI, the theoretical LOD of the digital immunomagnetic assay for clinical samples is expected to be limited mainly by equilibrium considerations and NSB.[37]

In this work, by combining the high sensitivity and high spatial resolution of NV sensor-based magnetic imaging under ambient conditions, we proposed and experimentally realized a digital magnetic method for general biomolecular interactions. The method has the advantages of low signal background, high signal stability, the ability of magnetic purification and enrichment, and accurate quantification. It opens the door to single-molecule or ultrasensitive magnetometry for biomolecular interaction research, highly sensitive clinical diagnostics, and drug screening.

To study cellular biomolecular interactions, particularly protein−protein interactions, inspired by conventional coimmunoprecipitation (Co-IP) and pull-down examinations,[1] the SPIMA in the present work can be evolved into a single-particle Co-IP or pull-down approach, enabling us to study physiological protein interactions with single-molecule sensitivity and requiring much fewer samples, even a single cell. Then, NV centers are highly sensitive to the spatiotemporal changes of a magnetic field.[19] Thus, in a physiological solution, single-molecule interactions could be magnetically monitored in real time by SiPMI for a long time to analyze the dynamics and even manipulated by an external magnetic field. This single-molecule magnetometry would provide new opportunities for biomolecular structure and function research. In addition, for clinical diagnostics, by combining with microfluidics and LFA toolkits, the SPIMA can be further developed into a general ultrasensitive immunoassay approach for assays of a broad range of analytes, including proteins, nucleic acids, viruses, extracellular vesicles, and circulating tumor cells.

In future studies, several technical improvements will contribute to more efficient SiPMI detection and meet the extended applications described above. The first is to improve the sensitivity and efficiency of magnetic imaging by using an isotope-C_{12} enriched diamond sensor and lock-in detection technique, increasing the NV center density, and optimizing the thickness of the NV layer.[47] Optimizing the functionalization and depositing suitable atomic layers such as the Al_2O_3 layer[38] or SiO_2 layer on the diamond surface could increase the effective binding sites of the surface, which would contribute to SiPMI detection sensitivity. In addition, fabricating a nanopillar array on diamond will facilitate the single-molecule magnetic detection. Lastly, the use of a diamond chip with multiple functional areas, a multichannel microfluidic chip, a functionalized membrane, or a test strip will enable parallel SiPMI examination of a large number of biomedical samples and multiple factors in a single sample.

■ ASSOCIATED CONTENT

Supporting Information

The Supporting Information is available free of charge at https://pubs.acs.org/doi/10.1021/acs.nanolett.2c04961.

Experimental section; simulation of single-particle magnetic fields; deep learning model; fluorescence images of fluorescence-labeled biomolecules and MNPs on diamonds; the stability of magnetic signals and fluorescent signals; nonspecific adsorption of DNA on the diamond surface and passivation treatments; SPIMA results of clinical serum samples; parameters of the deep learning training set; DNA primers (PDF)

■ AUTHOR INFORMATION

Corresponding Authors

Fazhan Shi − *CAS Key Laboratory of Microscale Magnetic Resonance and School of Physical Sciences, University of Science and Technology of China, Hefei 230026, China; CAS Center for Excellence in Quantum Information and Quantum Physics, University of Science and Technology of China, Hefei 230026, China; School of Biomedical Engineering and Suzhou Institute for Advanced Research, University of Science and Technology of China, Suzhou 215123, China; Hefei National Laboratory, University of Science and Technology of China, Hefei 230088, China*; Email: fzshi@ustc.edu.cn

Jiangfeng Du − *CAS Key Laboratory of Microscale Magnetic Resonance and School of Physical Sciences, University of Science and Technology of China, Hefei 230026, China; CAS Center for Excellence in Quantum Information and Quantum Physics, University of Science and Technology of China, Hefei 230026, China; Hefei National Laboratory, University of Science and Technology of China, Hefei 230088, China*; orcid.org/0000-0001-8085-8012; Email: djf@ustc.edu.cn

Authors

Sanyou Chen − *CAS Key Laboratory of Microscale Magnetic Resonance and School of Physical Sciences, University of Science and Technology of China, Hefei 230026, China; CAS Center for Excellence in Quantum Information and Quantum Physics, University of Science and Technology of China, Hefei 230026, China; School of Biomedical Engineering and Suzhou Institute for Advanced Research, University of Science and Technology of China, Suzhou 215123, China*; orcid.org/0000-0002-0285-3416

Ziting Sun − *CAS Key Laboratory of Microscale Magnetic Resonance and School of Physical Sciences, University of Science and Technology of China, Hefei 230026, China; CAS Center for Excellence in Quantum Information and Quantum Physics, University of Science and Technology of China, Hefei 230026, China*

https://doi.org/10.1021/acs.nanolett.2c04961
Nano Lett. 2023, 23, 2636−2643

Wanhe Li − *CAS Key Laboratory of Microscale Magnetic Resonance and School of Physical Sciences, University of Science and Technology of China, Hefei 230026, China; CAS Center for Excellence in Quantum Information and Quantum Physics, University of Science and Technology of China, Hefei 230026, China*

Pei Yu − *CAS Key Laboratory of Microscale Magnetic Resonance and School of Physical Sciences, University of Science and Technology of China, Hefei 230026, China; CAS Center for Excellence in Quantum Information and Quantum Physics, University of Science and Technology of China, Hefei 230026, China*

Qian Shi − *CAS Key Laboratory of Microscale Magnetic Resonance and School of Physical Sciences, University of Science and Technology of China, Hefei 230026, China; CAS Center for Excellence in Quantum Information and Quantum Physics, University of Science and Technology of China, Hefei 230026, China*

Fei Kong − *CAS Key Laboratory of Microscale Magnetic Resonance and School of Physical Sciences, University of Science and Technology of China, Hefei 230026, China; CAS Center for Excellence in Quantum Information and Quantum Physics, University of Science and Technology of China, Hefei 230026, China*

Qi Zhang − *CAS Key Laboratory of Microscale Magnetic Resonance and School of Physical Sciences, University of Science and Technology of China, Hefei 230026, China; CAS Center for Excellence in Quantum Information and Quantum Physics, University of Science and Technology of China, Hefei 230026, China; School of Biomedical Engineering and Suzhou Institute for Advanced Research, University of Science and Technology of China, Suzhou 215123, China;* orcid.org/0000-0001-8889-2039

Pengfei Wang − *CAS Key Laboratory of Microscale Magnetic Resonance and School of Physical Sciences, University of Science and Technology of China, Hefei 230026, China; CAS Center for Excellence in Quantum Information and Quantum Physics, University of Science and Technology of China, Hefei 230026, China; Hefei National Laboratory, University of Science and Technology of China, Hefei 230088, China;* orcid.org/0000-0001-5112-0502

Ya Wang − *CAS Key Laboratory of Microscale Magnetic Resonance and School of Physical Sciences, University of Science and Technology of China, Hefei 230026, China; CAS Center for Excellence in Quantum Information and Quantum Physics, University of Science and Technology of China, Hefei 230026, China; Hefei National Laboratory, University of Science and Technology of China, Hefei 230088, China;* orcid.org/0000-0001-6232-7234

Complete contact information is available at: https://pubs.acs.org/10.1021/acs.nanolett.2c04961

Author Contributions

#S.C., Z.S., W.L., and P.Y. contributed equally to this work. J.D. and F.S. supervised the project. J.D., F.S., and S.C. proposed the idea and designed the experiments. Z.S., W.L., and S.C. built the diamond magnetic microscope. P.Y. and Y.W. fabricated the diamond sensors. Z.S., W.L., and Q.S. simulated and reconstructed the magnetic signals. Z.S., S.C., Q.S., and F.S. performed the experiments. S.C., Z.S., and F.S. carried out the data analysis. F.K., Q.Z., and P.W. provided the technical support. S.C., Z.S., F.S., and J.D. wrote the manuscript. All authors analyzed the data, discussed the results, and commented on the manuscript.

Notes

The authors declare no competing financial interest.

■ ACKNOWLEDGMENTS

We thank Tengchuan Jin (University of Science and Technology of China) for providing human serum samples. The fabrication of diamond sensors was performed at the USTC Center for Micro and Nanoscale Research and Fabrication. This work was supported by the National Natural Science Foundation of China (grant nos. T2125011, 32071450, 81788101), the National Key R&D Program of China (grant nos. 2018YFA0306600, 2021YFB3202800, 2019YFA0709300, 2016YFA0502400), the CAS (grant nos. YSBR-068, XDC07000000, GJJSTD20200001, YIPA2015370), the Innovation Program for Quantum Science and Technology (grant no. 2021ZD0303204), the Anhui Initiative in Quantum Information Technologies (grant no. AHY050000), the Hefei Comprehensive National Science Center, and the Fundamental Research Funds for the Central Universities.

■ REFERENCES

(1) Rao, V. S.; Srinivas, K.; Sujini, G. N.; Kumar, G. N. Protein-protein interaction detection: methods and analysis. *Int. J. Proteomics* **2014**, *2014*, 147648.

(2) Xing, S.; Wallmeroth, N.; Berendzen, K. W.; Grefen, C. Techniques for the Analysis of Protein-Protein Interactions in Vivo. *Plant Physiol* **2016**, *171*, 727−758.

(3) Ramanathan, M.; Porter, D. F.; Khavari, P. A. Methods to study RNA-protein interactions. *Nat. Methods* **2019**, *16*, 225−234.

(4) Altug, H.; Oh, S. H.; Maier, S. A.; Homola, J. Advances and applications of nanophotonic biosensors. *Nat. Nanotechnol* **2022**, *17*, 5−16.

(5) Nguyen, H. H.; Park, J.; Kang, S.; Kim, M. Surface plasmon resonance: a versatile technique for biosensor applications. *Sensors (Basel)* **2015**, *15*, 10481−10510.

(6) Concepcion, J.; Witte, K.; Wartchow, C.; Choo, S.; Yao, D. F.; Persson, H.; Wei, J.; Li, P.; Heidecker, B.; Ma, W. L.; Varma, R.; Zhao, L. S.; Perillat, D.; Carricato, G.; Recknor, M.; Du, K.; Ho, H.; Ellis, T.; Gamez, J.; Howes, M.; Phi-Wilson, J.; Lockard, S.; Zuk, R.; Tan, H. Label-Free Detection of Biomolecular Interactions Using BioLayer Interferometry for Kinetic Characterization. *Comb Chem. High T Scr* **2009**, *12*, 791−800.

(7) Lerner, E.; Cordes, T.; Ingargiola, A.; Alhadid, Y.; Chung, S.; Michalet, X.; Weiss, S. Toward dynamic structural biology: Two decades of single-molecule Forster resonance energy transfer. *Science* **2018**, *359*, No. eaan1133.

(8) Jain, A.; Liu, R.; Ramani, B.; Arauz, E.; Ishitsuka, Y.; Ragunathan, K.; Park, J.; Chen, J.; Xiang, Y. K.; Ha, T. Probing cellular protein complexes using single-molecule pull-down. *Nature* **2011**, *473*, 484−488.

(9) Neuman, K. C.; Nagy, A. Single-molecule force spectroscopy: optical tweezers, magnetic tweezers and atomic force microscopy. *Nat. Methods* **2008**, *5*, 491−505.

(10) Thakur, A. K.; Movileanu, L. Real-time measurement of protein-protein interactions at single-molecule resolution using a biological nanopore. *Nat. Biotechnol.* **2019**, *37*, 96−101.

(11) Colombo, M.; Carregal-Romero, S.; Casula, M. F.; Gutierrez, L.; Morales, M. P.; Bohm, I. B.; Heverhagen, J. T.; Prosperi, D.; Parak, W. J. Biological applications of magnetic nanoparticles. *Chem. Soc. Rev.* **2012**, *41*, 4306−4334.

(12) Issadore, D.; Park, Y. I.; Shao, H.; Min, C.; Lee, K.; Liong, M.; Weissleder, R.; Lee, H. Magnetic sensing technology for molecular analyses. *Lab Chip* **2014**, *14*, 2385−2397.

(13) Murzin, D.; Mapps, D. J.; Levada, K.; Belyaev, V.; Omelyanchik, A.; Panina, L.; Rodionova, V. Ultrasensitive Magnetic Field Sensors for Biomedical Applications. *Sensors (Basel)* **2020**, *20*, 1569.
(14) Su, D.; Wu, K.; Saha, R.; Peng, C.; Wang, J. P. Advances in Magnetoresistive Biosensors. *Micromachines (Basel)* **2020**, *11*, 34.
(15) Gaster, R. S.; Xu, L.; Han, S. J.; Wilson, R. J.; Hall, D. A.; Osterfeld, S. J.; Yu, H.; Wang, S. X. Quantification of protein interactions and solution transport using high-density GMR sensor arrays. *Nat. Nanotechnol* **2011**, *6*, 314−20.
(16) Schirhagl, R.; Chang, K.; Loretz, M.; Degen, C. L. Nitrogen-vacancy centers in diamond: nanoscale sensors for physics and biology. *Annu. Rev. Phys. Chem.* **2014**, *65*, 83−105.
(17) Balasubramanian, G.; Chan, I. Y.; Kolesov, R.; Al-Hmoud, M.; Tisler, J.; Shin, C.; Kim, C.; Wojcik, A.; Hemmer, P. R.; Krueger, A.; Hanke, T.; Leitenstorfer, A.; Bratschitsch, R.; Jelezko, F.; Wrachtrup, J. Nanoscale imaging magnetometry with diamond spins under ambient conditions. *Nature* **2008**, *455*, 648−651.
(18) Maze, J. R.; Stanwix, P. L.; Hodges, J. S.; Hong, S.; Taylor, J. M.; Cappellaro, P.; Jiang, L.; Dutt, M. V.; Togan, E.; Zibrov, A. S.; Yacoby, A.; Walsworth, R. L.; Lukin, M. D. Nanoscale magnetic sensing with an individual electronic spin in diamond. *Nature* **2008**, *455*, 644−647.
(19) Barry, J. F.; Turner, M. J.; Schloss, J. M.; Glenn, D. R.; Song, Y.; Lukin, M. D.; Park, H.; Walsworth, R. L. Optical magnetic detection of single-neuron action potentials using quantum defects in diamond. *Proc. Natl. Acad. Sci. U.S.A.* **2016**, *113*, 14133−14138.
(20) Xie, Y. J.; Yu, H. Y.; Zhu, Y. B.; Qin, X.; Rong, X.; Duan, C. K.; Du, J. F. A hybrid magnetometer towards femtotesla sensitivity under ambient conditions. *Sci. Bull.* **2021**, *66*, 127−132.
(21) Zhang, C.; Shagieva, F.; Widmann, M.; Kubler, M.; Vorobyov, V.; Kapitanova, P.; Nenasheva, E.; Corkill, R.; Rhrle, O.; Nakamura, K.; Sumiya, H.; Onoda, S.; Isoya, J.; Wrachtrup, J. Diamond Magnetometry and Gradiometry Towards Subpicotesla dc Field Measurement. *Physical Review Applied* **2021**, *15*, 064075.
(22) Shi, F.; Zhang, Q.; Wang, P.; Sun, H.; Wang, J.; Rong, X.; Chen, M.; Ju, C.; Reinhard, F.; Chen, H.; Wrachtrup, J.; Wang, J.; Du, J. Protein imaging. Single-protein spin resonance spectroscopy under ambient conditions. *Science* **2015**, *347*, 1135−1138.
(23) Lovchinsky, I.; Sushkov, A. O.; Urbach, E.; de Leon, N. P.; Choi, S.; De Greve, K.; Evans, R.; Gertner, R.; Bersin, E.; Muller, C.; McGuinness, L.; Jelezko, F.; Walsworth, R. L.; Park, H.; Lukin, M. D. Nuclear magnetic resonance detection and spectroscopy of single proteins using quantum logic. *Science* **2016**, *351*, 836−841.
(24) Shi, F.; Kong, F.; Zhao, P.; Zhang, X.; Chen, M.; Chen, S.; Zhang, Q.; Wang, M.; Ye, X.; Wang, Z.; Qin, Z.; Rong, X.; Su, J.; Wang, P.; Qin, P. Z.; Du, J. Single-DNA electron spin resonance spectroscopy in aqueous solutions. *Nat. Methods* **2018**, *15*, 697−699.
(25) Le Sage, D.; Arai, K.; Glenn, D. R.; DeVience, S. J.; Pham, L. M.; Rahn-Lee, L.; Lukin, M. D.; Yacoby, A.; Komeili, A.; Walsworth, R. L. Optical magnetic imaging of living cells. *Nature* **2013**, *496*, 486−489.
(26) Glenn, D. R.; Lee, K.; Park, H.; Weissleder, R.; Yacoby, A.; Lukin, M. D.; Lee, H.; Walsworth, R. L.; Connolly, C. B. Single-cell magnetic imaging using a quantum diamond microscope. *Nat. Methods* **2015**, *12*, 736−738.
(27) Wang, P.; Chen, S.; Guo, M.; Peng, S.; Wang, M.; Chen, M.; Ma, W.; Zhang, R.; Su, J.; Rong, X.; Shi, F.; Xu, T.; Du, J. Nanoscale magnetic imaging of ferritins in a single cell. *Sci. Adv.* **2019**, *5*, No. eaau8038.
(28) Chen, S.; Li, W.; Zheng, X.; Yu, P.; Wang, P.; Sun, Z.; Xu, Y.; Jiao, D.; Ye, X.; Cai, M.; Shen, M.; Wang, M.; Zhang, Q.; Kong, F.; Wang, Y.; He, J.; Wei, H.; Shi, F.; Du, J. Immunomagnetic microscopy of tumor tissues using quantum sensors in diamond. *Proc. Natl. Acad. Sci. U.S.A.* **2022**, *119*, No. e2118876119.
(29) Davis, H. C.; Ramesh, P.; Bhatnagar, A.; Lee-Gosselin, A.; Barry, J. F.; Glenn, D. R.; Walsworth, R. L.; Shapiro, M. G. Mapping the microscale origins of magnetic resonance image contrast with subcellular diamond magnetometry. *Nat. Commun.* **2018**, *9*, 131.
(30) Kayci, M.; Fan, J.; Bakirman, O.; Herrmann, A. Multiplexed sensing of biomolecules with optically detected magnetic resonance of nitrogen-vacancy centers in diamond. *Proc. Natl. Acad. Sci. U.S.A.* **2021**, *118*, No. e2112664118.
(31) Gould, M.; Barbour, R. J.; Thomas, N.; Arami, H.; Krishnan, K. M.; Fu, K. M. C. Room-temperature detection of a single 19 nm super-paramagnetic nanoparticle with an imaging magnetometer. *Appl. Phys. Lett.* **2014**, *105*, 072406.
(32) McCoey, J. M.; de Gille, R. W.; Nasr, B.; Tetienne, J. P.; Hall, L. T.; Simpson, D. A.; Hollenberg, L. C. L. Rapid, High-Resolution Magnetic Microscopy of Single Magnetic Microbeads. *Small* **2019**, *15*, 1805159.
(33) Lequin, R. M. Enzyme Immunoassay (EIA)/Enzyme-Linked Immunosorbent Assay (ELISA). *Clinical Chemistry* **2005**, *51*, 2415−2418.
(34) Rissin, D. M.; Kan, C. W.; Campbell, T. G.; Howes, S. C.; Fournier, D. R.; Song, L.; Piech, T.; Patel, P. P.; Chang, L.; Rivnak, A. J.; Ferrell, E. P.; Randall, J. D.; Provuncher, G. K.; Walt, D. R.; Duffy, D. C. Single-molecule enzyme-linked immunosorbent assay detects serum proteins at subfemtomolar concentrations. *Nat. Biotechnol.* **2010**, *28*, 595−599.
(35) Liu, Y. L.; Zhan, L.; Qin, Z. P.; Sackrison, J.; Bischof, J. C. Ultrasensitive and Highly Specific Lateral Flow Assays for Point-of-Care Diagnosis. *ACS Nano* **2021**, *15*, 3593−3611.
(36) Wang, T.-C.; Liu, M.-Y.; Zhu, J.-Y.; Tao, A.; Kautz, J.; Catanzaro, B. High-Resolution Image Synthesis and Semantic Manipulation with Conditional GANs. In *Proceedings of the IEEE Conference on Computer Vision and Pattern Recognition (CVPR)*, Salt Lake City, UT, 2018; pp 8798−8807.
(37) Frutiger, A.; Tanno, A.; Hwu, S.; Tiefenauer, R. F.; Voros, J.; Nakatsuka, N. Nonspecific Binding-Fundamental Concepts and Consequences for Biosensing Applications. *Chem. Rev.* **2021**, *121*, 8095−8160.
(38) Xie, M.; Yu, X.; Rodgers, L. V. H.; Xu, D.; Chi-Duran, I.; Toros, A.; Quack, N.; de Leon, N. P.; Maurer, P. C. Biocompatible surface functionalization architecture for a diamond quantum sensor. *Proc. Natl. Acad. Sci. U.S.A.* **2022**, *119*, No. e2114186119.
(39) Minchin, S.; Lodge, J. Understanding biochemistry: structure and function of nucleic acids. *Essays Biochem* **2019**, *63*, 433−456.
(40) Li, M.; Yin, F.; Song, L.; Mao, X.; Li, F.; Fan, C.; Zuo, X.; Xia, Q. Nucleic Acid Tests for Clinical Translation. *Chem. Rev.* **2021**, *121*, 10469−10558.
(41) Wierucka, M.; Biziuk, M. Application of magnetic nanoparticles for magnetic solid-phase extraction in preparing biological, environmental and food samples. *TrAC Trends in Analytical Chemistry* **2014**, *59*, 50−58.
(42) Cohen, L.; Walt, D. R. Highly Sensitive and Multiplexed Protein Measurements. *Chem. Rev.* **2019**, *119*, 293−321.
(43) Cretich, M.; Daaboul, G. G.; Sola, L.; Unlu, M. S.; Chiari, M. Digital detection of biomarkers assisted by nanoparticles: application to diagnostics. *Trends Biotechnol* **2015**, *33*, 343−351.
(44) Belushkin, A.; Yesilkoy, F.; Gonzalez-Lopez, J. J.; Ruiz-Rodriguez, J. C.; Ferrer, R.; Fabrega, A.; Altug, H. Rapid and Digital Detection of Inflammatory Biomarkers Enabled by a Novel Portable Nanoplasmonic Imager. *Small* **2020**, *16*, No. e1906108.
(45) Duffy, D. C. Digital detection of proteins. *Lab Chip* **2023**, *23*, 818−847.
(46) Carter, L. J.; Garner, L. V.; Smoot, J. W.; Li, Y. Z.; Zhou, Q. Q.; Saveson, C. J.; Sasso, J. M.; Gregg, A. C.; Soares, D. J.; Beskid, T. R.; Jervey, S. R.; Liu, C. Assay Techniques and Test Development for COVID-19 Diagnosis. *ACS Central Sci.* **2020**, *6*, 591−605.
(47) Levine, E. V.; Turner, M. J.; Kehayias, P.; Hart, C. A.; Langellier, N.; Trubko, R.; Glenn, D. R.; Fu, R. R.; Walsworth, R. L. Principles and techniques of the quantum diamond microscope. *Nanophotonics-Berlin* **2019**, *8*, 1945−1973.

https://doi.org/10.1021/acs.nanolett.2c04961
Nano Lett. 2023, 23, 2636−2643